Novel X-ray Detection Scheme for Small-angle Scattering Tomography

*Guang Li, Wenxiang Cong, James S. Michaelson, Hong Liu and Ge Wang**

Abstract — The state of the art micro-CT scanner plays an indispensable role in examining small animals and various samples. For example, surgical specimens can be scanned to find positive tumor margins. However, most of available micro-CT systems are of general types, and suffer from a poor soft tissue contrast. In this paper, we propose a new detector design dedicated to capture small-angle scattering signals only, which carry critical pathological information for differentiation between benign and malignant tumors. Our design consists of two interlaced gratings so that both the primary flux and Compton scattering photons are effectively blocked to leave the apertures mainly open to small-angle scattering photons. By theoretical analysis and Monte Carlo simulation, it is demonstrated that with our proposed techniques small-angle scattering signals can be detected for image reconstruction.

Index Terms — X-ray micro-CT, small-angle scattering, grating based x-ray imaging, pathological studies.

I. Introduction

Now there have been many varieties of commercial micro-CT scanners for various applications [1-3]. With the development of X-ray source, detector and reconstruction techniques, the spatial resolution and temporal resolution of micro-CT have been significantly improved. Because of these improvements, micro-CT becomes more powerful and more indispensable especially in preclinical studies. Recently, micro-CT has been evaluated to image cancer specimens and test their margin positivity.

At present, most of commercial micro-CT scanners have utilized only one contrast mechanism, which is known as x-ray linear attenuation. Consequently, micro-CT has a poor soft tissue contrast. Indeed, the x-ray attenuation coefficient is roughly proportional to the fourth power of the atomic number, and biological soft tissues are rather similar in terms of the atomic number. To address this disadvantage, researchers have been investigating alternative contrast mechanisms to enhance soft tissue features.

One popular option to improve micro-CT contrast resolution is to introduce contrast agents containing high-Z elements. A recent breakthrough is in grating-based x-ray phase-contrast and small-angle scattering imaging, which reveals subtle features of biological soft tissues. X-ray phase contrast imaging extracts phase shift information when x-ray waves travel through an object [4]. Small-angle scattering or dark-field imaging targets small-angle scattering signals governed by micro-scale structures of pathological relevance.

Although phase-contrast imaging has been studied since early 1990's, none of the classic techniques has the potential to be widely used until the emergence of x-ray grating-based interferometry or Talbot-Lau interferometry that works with a hospital-grade x-ray tube [5]. A Talbot-Lau interferometer simultaneously produces three types of reconstruction images in the attenuation, differential phase-contrast and dark-field modes respectively. Among these three images, small-angle scattering or dark-field images are of our primary interest, because they carry critical pathological information for differentiation between benign and malignant tumors. Several decades ago, scattering-based imaging, especially small-angle scattering imaging or spectroscopy, was already studied to reflect inner structures of an object at a molecular/cellular level [6-7]. Importantly, when cancer invades normal tissue, changes will be induced to molecular/cellular textures. These fine signatures directly affect small-angle scattering signals.

Conventionally, scattering-based imaging techniques perform slot scanning aided by collimators [8]. This kind of systems can get scattering signals at characteristic angles, but its scanning efficiency is very low. Currently, x-ray grating-based interferometry allows small-angle scattering imaging in cone-beam geometry, but the stepping procedure is sensitive and time-consuming. In this paper, we proposed a new dedicated small-angle scattering imaging technology composed of two interlaced gratings. The key idea behind our design is that both the primary X-rays and Compton scattering photons are basically blocked so that only small-angle scattering X-rays are admitted to go through the paired gratings and reach the detector behind the gratings.

In the rest of this paper, we first describe the theory and method in the second section. Then, we report our numerical results in the parallel beam geometry. In the last section, we discuss relevant issues and conclude the paper.

II. Theory and Method

2.1. Overall Setup

As our proposed small-angle scattering imaging scheme is new, we start with the parallel beam geometry to verify the feasibility. In the parallel-beam geometry, the schematic design is illustrated in Figure 1. The most important component in this system is the combination of two absorption gratings (red

Guang Li, Biomedical Imaging Center, BME/CBIS, Rensselaer Polytechnic Institute, New York, USA (e-mail: liguangeagle@126.com).

Wenxiang Cong, Biomedical Imaging Center, BME/CBIS, Rensselaer Polytechnic Institute, New York, USA (e-mail: congw@rpi.edu).

James S. Michaelson, Department of Pathology, Harvard Medical School, Massachusetts, USA (email: JamesMichaelsonPhD@gmail.com)

Hong Liu, Center for advanced medical imaging, University of Oklahoma, USA (email: liu@ou.edu)

Ge Wang, Biomedical Imaging Center, BME/CBIS, Rensselaer Polytechnic Institute, New York, USA (e-mail: wangg6@rpi.edu)

DOI: 10.12059/Fully3D.2017-11-3203020

columns in Figure 1) made of tungsten or lead. The duty cycle of each grating is 50%. The two gratings are complementary, and all the primary parallel x-rays are completely blocked, and only those rays that pass through the object and scattered at small/specific angles can be detected by the detector behind the gratings. Between the two layers, the gap can be used to modulate the incidence angle, and the septa (blue columns) in the gap prevent cross talks among neighboring cells.

2.2 Geometrical Parameters

Scattered photons are often considered as noise in practice as they randomly diffuse over the detector cells, and therefore cannot be extracted effectively. However, our proposed detection scheme can specifically extract small-angle scattering signals with appropriate geometrical parameters. All the key parameters are shown in Figure 2. Each cell of the grating contains two parts: solid part and hollow part. The height and width of each cell are h_1 and $2w_1$ respectively, and the widths of the solid part and the hollow part are all equal to w_1. The length of the gap between two layers is l_1. The pixel size of the detector is $2w_1$ for convenience, and thus one pixel covers one cell.

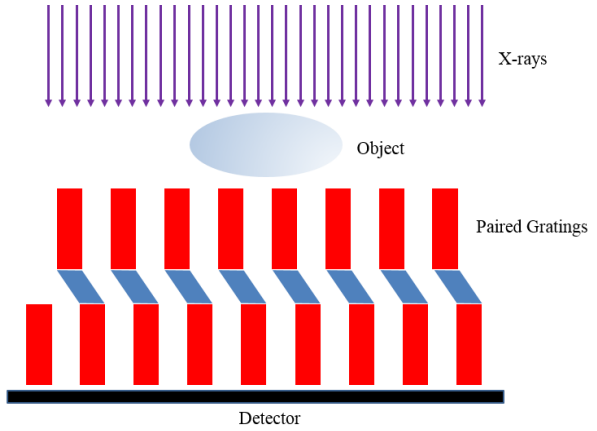

Figure 1. Schematic of the small-angle scattering imaging setup.

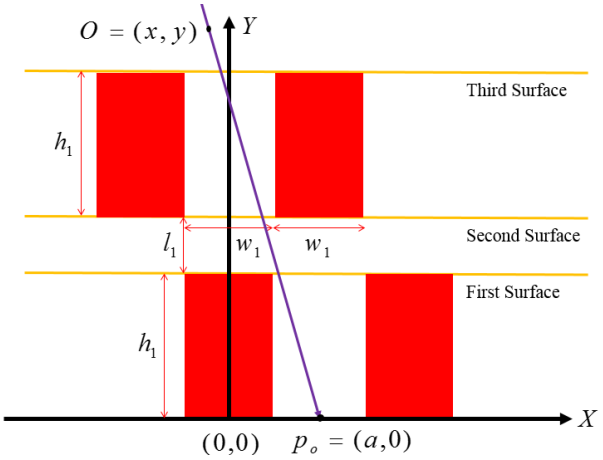

Figure 2. Geometrical parameters of the paired gratings.

In order to determine these parameters optimally, we first set up a rectangular coordinate system as shown in Figure 2. For a scattered photon from point $O=(x,y)$ to reach the point $p_o=(a,0)$ on the detector, it must go through the three surfaces shown in Figure 2 without hitting the grating metal, and the following four equations need to be simultaneously satisfied:

$$\begin{cases} \dfrac{w_1}{2} < a < \dfrac{3w_1}{2} \\ \dfrac{w_1}{2} < a + \dfrac{h_1(x-a)}{y} < \dfrac{3w_1}{2} \\ -\dfrac{w_1}{2} < a + \dfrac{(h_1+l_1)(x-a)}{y} < \dfrac{w_1}{2} \\ -\dfrac{w_1}{2} < a + \dfrac{(2h_1+l_1)(x-a)}{y} < \dfrac{w_1}{2} \end{cases} \tag{1}$$

By simplifying the set of equations (1), we can draw the conclusion that if $a > \dfrac{l_1+h_1}{h_1} w_1 + \dfrac{w_1}{2}$, the following relationship will hold

$$\frac{-\frac{w_1}{2}-a}{2h_1+l_1} y + a < x < \frac{\frac{w_1}{2}-a}{h_1+l_1} y + a \tag{2}$$

Otherwise, we have

$$\frac{\frac{w_1}{2}-a}{h_1} y + a < x < \frac{\frac{w_1}{2}-a}{h_1+l_1} y + a \tag{3}$$

Because $\dfrac{w_1}{2} < a < \dfrac{3w_1}{2}$, Eq. (3) will hold. From Eq. (3), we can derive the receiving range of the scattering angle at $p_o=(a,0)$ on the detector as

$$\arctan\frac{a-\frac{w_1}{2}}{h_1+l_1} < \theta < \arctan\frac{a-\frac{w_1}{2}}{h_1} \tag{4}$$

To further simplify Eq. (4), the receiving range of each pixel element can be expressed as

$$0 < \theta < \arctan\frac{w_1}{h_1} \tag{5}$$

According to the above analysis, next we will use the *EGSnrc* simulation system to perform Monte Carlo simulations to verify the feasibility of the proposed small-angle scattering imaging system.

III. Numerical Results

EGSnrc is a well-known simulation software whose function is to model the propagation of electrons and photons through matters. Because it relies on the Monte Carlo simulation, it is highly accurate. In our simulation, the grating was made of tungsten. The height and width of each grating cell were set to be 1cm and 0.5mm respectively. The dimensions of the detector were 100mm × 3mm with pixel size of 1mm. The length of the gap between the two gratings was 0.1cm. The x-ray source emitted a parallel beam of 1.28×10^{10} photons at an operating

voltage 20Kvp in each exposure. The cylindrical water phantom was used of radius 5mm and height 1mm.

In the first simulation, five copies of this phantom were put equi-spatially in front of the grating pair, very close to the top surface of the paired gratings as shown in Figure 3. The projection profile of the five phantoms was obtained along the middle line of the detector as shown in Figure 4.

It is clear that the five similar peaks correspond to the five circular phantoms. It can be observed in Figure 4 that all the peaks appear arcuate. According to the relationship between the incident flux and the small angle scattering intensity [9]:

$$P_1 = I_0 \sigma(0) t \Omega \exp(-\mu t) \qquad (6)$$

where I_0 is the incident flux, $\sigma(0)$ is the scattering coefficient in the forward direction per unit solid angle per unit thickness of a sample, t is the sample thickness, Ω is the solid angle spanned by a detector element, μ is the linear attenuation coefficient. Hence, the scattering intensity should be roughly proportional to the distance over which the x-ray beam goes through the phantom, and the peaks in Figure 4 are indeed consistent with this approximation, and the width of each peak is the same as the diameter of the phantom.

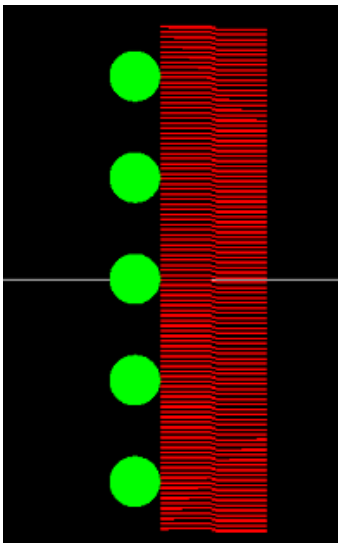

Figure 3. Diagram of the phantoms and the gratings in the first simulation.

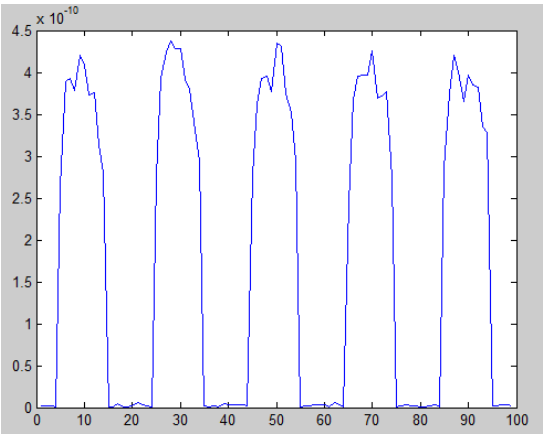

Figure 4. Projection data along the middle line of the detector.

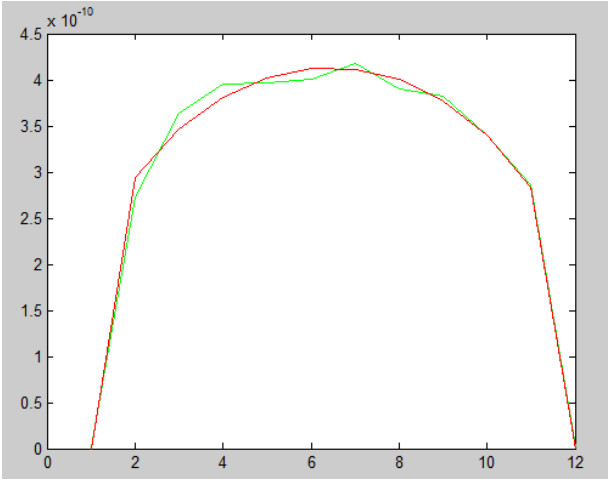

Figure 5. Average from ten groups of small-angle scattering profiles (green) and its quadratic fitting (red).

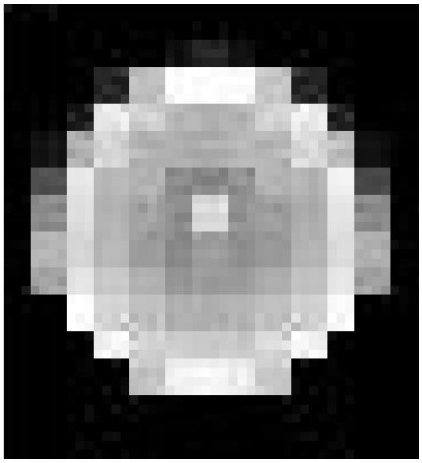

Figure 6. Reconstructed image from small-angle scattering data.

In the second simulation, there was only one cylindrical phantom located in front of the pair of the gratings. In order to reconstruct an image from small-angle scattering data, the phantom was rotated over a range of 360˚ equiangularly around its center and 10 groups of scattering data were acquired. The average value of these 10 groups of data is in Figure 5 (green curve). It can be seen that the quadratic fit curve (red line) worked well with the simulated profile, which means that the scattering signal matched Eq. (6) quite well. According to our physical model for small-angle x-ray scattering derived from the principle of energy conservation [10], we used these ten groups of scattering data to reconstruct the cross-sectional image as shown in Figure 6. The shape and size of the disk in Figure 6 are in agreement with those of the phantom. This result demonstrates that the proposed small-angle scattering imaging system can acquire small angle scattering data for image reconstruction. In order to evaluate the image resolution of our proposed system, we simulated a hollow cylindrical water phantom and put it in front of the paired gratings as shown in Figure 7(a), and the corresponding scattering signal was plotted in Figure 7(b). In contrast to the profile in Figure 5, the profile in Figure 7(b) shows an indent corresponding to the inner hole of the phantom.

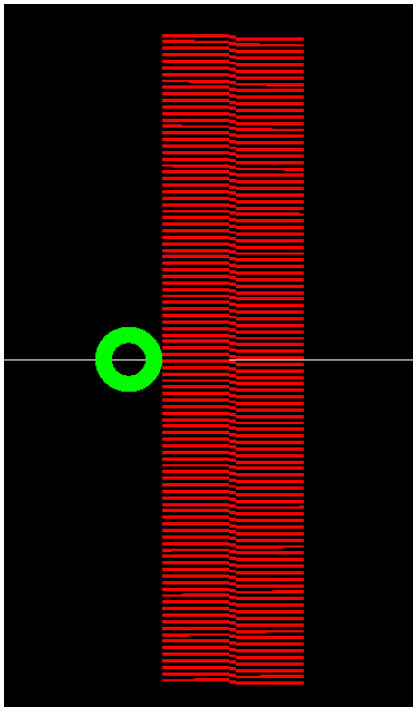

(a)

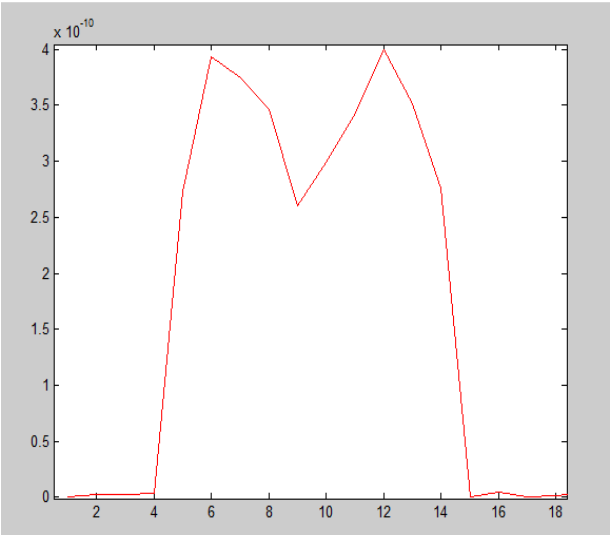

(b)

Figure 7. Hollow cylindrical water phantom and its small-angle scattering profile.

IV. Discussions and Conclusion

By theoretical analysis and Monte Carlo simulation, we have demonstrated that the proposed setup can perform well in parallel beam geometry for small-angle scattering imaging. In fan beam and cone beam geometry, the system needs to be modified with conformable geometrical shapes and parameters of the gratings. Other types of paired gratings can be also designed in the same spirit of our reported work.

For image reconstruction, how to model the formation of small-angle scattering signals remains an interesting question. Despite the availability of several models such as Eq. (6) and [10], further refinements can be certainly done. Eventually, small-angle scattering tensor tomography should be also possible.

The magnitude of small angle scattering signals is very small, and we are very interested in finding how to improve the data acquisition efficiency. One way is to modify gratings and innovate detectors for practical applications. Another way is to use bright an x-ray source such as a Thomson scattering x-ray source.

Pathologically, small-angle scattering imaging can provide more sensitive and specific information about surgical specimens, and guide surgical procedures on spot. Our proposed technology should be robust and cost-effective. Hence, we are interested in developing the technology further and prototyping it as a novel tool for niche clinical and preclinical applications.

In summary, we have proposed a new small-angle scattering imaging system featured by a pair of complementary x-ray gratings. This approach is focused on small-angle scattering signal detection, involves no mechanical stepping, and should be practical if it is fully developed. We are actively working along this direction, and will report more results in the future.

Acknowledgments

This work is partially supported by NIH/NIBIB National Institutes of Health Grant R01 EB016977.

References

[1] M. J. Paulus, S. S. Gleason, S. J. Kennel, P. R. Hunsicker, and D. K. Johnson, "High resolution X-ray computed tomography: an emerging tool for small animal cancer research," *Neoplasia*, vol. 2, pp. 62-70, 2000.

[2] M. Ding, A. Odgaard, and I. Hvid, "Accuracy of cancellous bone volume fraction measured by micro-CT scanning," *Journal of biomechanics*, vol. 32, pp. 323-326, 1999.

[3] C. T. Badea, S. M. Johnston, Y. Qi, and G. A. Johnson, "4D micro-CT for cardiac and perfusion applications with view under sampling," *Physics In Medicine And Biology*, vol. 56, pp. 3351-3369, Jun 2011.

[4] A. Momose, T. Takeda, Y. Itai, and K. Hirano, "Phase–contrast X–ray computed tomography for observing biological soft tissues," *Nature medicine*, vol. 2, pp. 473-475, 1996.

[5] F. Pfeiffer, M. Bech, O. Bunk, P. Kraft, E. F. Eikenberry, C. Brönnimann, *et al.*, "Hard-X-ray dark-field imaging using a grating interferometer," *Nature materials*, vol. 7, pp. 134-137, 2008.

[6] S. Sidhu, G. Falzon, S. Hart, J. Fox, R. Lewis, and K. Siu, "Classification of breast tissue using a laboratory system for small-angle x-ray scattering (SAXS)," *Physics in medicine and biology*, vol. 56, p. 6779, 2011.

[7] J. Feldkamp, M. Kuhlmann, S. Roth, A. Timmann, R. Gehrke, I. Shakhverdova, *et al.*, "Recent developments in tomographic small angle X-ray scattering," *physica status solidi (a)*, vol. 206, pp. 1723-1726, 2009.

[8] K. Kern, L. Peerzada, L. Hassan, and C. MacDonald, "Design for a coherent-scatter imaging system compatible with screening mammography," *Journal of Medical Imaging*, vol. 3, pp. 030501-030501, 2016.

[9] N. Chonacky and W. Beeman, "The X-ray forward scattering coefficient of water," *Acta Crystallographica Section A: Crystal Physics, Diffraction, Theoretical and General Crystallography*, vol. 25, pp. 564-568, 1969.

[10] W. Cong, F. Pfeiffer, M. Bech, and G. Wang, "X-ray dark-field imaging modeling," *JOSA A*, vol. 29, pp. 908-912, 2012.